Progress In Electromagnetics Research B, Vol. 2, 259–278, 2008

MICROSTRIP ANTENNA WITH CORRUGATED GROUND PLANE SURFACE AS A SENSOR FOR LANDMINES DETECTION

S. H. Zainud-Deen, M. E. Badr, E. El-Deen, K. H. Awadalla and H. A. Sharshar

Faculty of Electronic Engineering
Menoufia University
Menouf, Egypt

Abstract—A proposed sensor for landmines detection consists of two parallel microstrip antennas placed on the same ground plane and with corrugated ground surface between the arrays has been investigated. The microstrip patch array with corrugated ground surface has the advantage of a low mutual coupling compared with the classic arrays. The Finite-Difference Time-Domain (FDTD) is used to simulate the sensor for landmines detection.

1. INTRODUCTION

Landmines affect at least 60 countries and injure or kill between 15,000 and 20,000 people annually. Mines are often buried or hidden so as not to be detected and may be laid in regular patterns around a village, along a road, on bridges, near single trees or along river blanks. There are two types of mine clearance, military and humanitarian. Military mine clearance is the process undertaken by solders to clear a safe path so that they can advance during the conflict. Humanitarian mine clearance is very difficult. It aims to clear land so that civilians can return to their homes and their every day routines without the threat of landmines and unexploded remnants of war. This means that all mines affecting the places where ordinary people live must be cleared, and their safety in areas that have been cleared must be guaranteed [1, 2].

Recent straggle in foreign lands have highlighted the need for effective mine location sensors. An effective sensor pinpoints the mine location with a very high probability of detection and very low false alarm rate. The mines encountered today come in a plethora of size and material and are buried at various depths, in various types of soil

land under various conditions. Thus, an important requirement for an electromagnetic sensor (Ground penetrating radars) operating at a radio or microwave frequency is the ability to detect all-dielectric (nonmetallic) mines, even in situations where the electrical properties (specifically the relative permittivity) of the mine are close to those of the surrounding soil [3–6]. Electromagnetic sensors use signals at radio and microwave frequencies for this purpose. A separated-aperture sensor, which consists of two parallel dipole antennas housed in corner reflectors that are separated by a metallic septum, has been investigated in [7–9]. Using the mutual coupling behavior between the two dipoles the presence of a buried target is determined. Recently two patch array antennas have been proposed for the detection of buried land mines [10, 11].

The patch antennas excite surface waves, which are guided by the substrate and the ground plane. Different efficient techniques have been investigated for reducing the mutual coupling between element arrays [11–13]. Recently new ground planes are introduced to electromagnetic called artificially soft ground plane, high impedance grounds, or perfect magnetic conductor (PMC) [14, 15]. The high impedance ground plane is a metal sheet with a two dimensional periodic resonant texture that suppresses surface waves in a desired frequency range called the band gap.

In this paper, a proposed sensor for landmines detection consists of two parallel microstrip antennas placed on the same ground plane with corrugated ground surface between the arrays has been investigated. A finite-difference time-domain (FDTD) program developed by the authors is used in the analysis. A brief analysis is shown in Section 2, the numerical results are given in Section 3, and the conclusions are given in Section 4.

2. PROBLEM FORMULATIONS

The FDTD method has firmly established itself as one of the most popular methods in computational electromagnetic, because of the increasing interest of modeling inhomogeneous materials. In 1966, Yee [16] first described a space-grid time-domain numerical technique for the solution of Maxwell's curl equations. The algorithm was based on a central-difference solution of Maxwell's curl equations with spatially staggered electric and magnetic field solved alternatively at each time step in a leap-frog algorithm. For linearly, isotropic and non-dispersive medium, the time-dependent Maxwell's equations can

be written as [17]:

$$\nabla x\bar{E} = -\mu\frac{\partial\bar{H}}{\partial t} - \sigma^*\bar{H} \tag{1}$$

$$\nabla x\bar{H} = \varepsilon\frac{\partial\bar{E}}{\partial t} + \sigma\bar{E} \tag{2}$$

where

$\bar{E}$: Electric field intensity (Volt/meter),

$\bar{H}$: Magnetic field intensity (Ampere/meter),

σ: Electric conductivity (Siemens/meter),

σ^*: Equivalent magnetic loss (Ohms/meter),

ε: Electrical permittivity (Farad/meter),

μ: Magnetic permeability (Henry/meter).

Yee discretized the space of the problem to small cubical cells and for each cell he locates the six field components to match the curl equations. The electric field vectors are located at the centre of the cube edges and parallel to the cube edges, while the magnetic field vectors are located at the centre of the cube faces and normal to the cube faces. The partial derivatives with respect to the space and time can be approximated using the central difference approximation. The six update equations of the magnetic and electric field components can be written as:

$$\begin{aligned} H_x^{n+1/2}(i,j,k) &= \frac{1-\sigma^*\Delta t/2\mu}{1+\sigma^*\Delta t/2\mu}H_x^{n-1/2}(i,j,k) \\ &\quad + \frac{\Delta t/\mu}{1+\sigma^*\Delta t/2\mu}\left[\frac{E_y^n(i,j,k+1)-E_y^n(i,j,k)}{\Delta z}\right. \\ &\quad \left. -\frac{E_z^n(i,j+1,k)-E_z^n(i,j,k)}{\Delta y}\right] \end{aligned} \tag{3}$$

$$\begin{aligned} H_y^{n+1/2}(i,j,k) &= \frac{1-\sigma^*\Delta t/2\mu}{1+\sigma^*\Delta t/2\mu}H_y^{n-1/2}(i,j,k) \\ &\quad + \frac{\Delta t/\mu}{1+\sigma^*\Delta t/2\mu}\left[\frac{E_z^n(i+1,j,k)-E_z^n(i,j,k)}{\Delta x}\right. \\ &\quad \left. -\frac{E_x^n(i,j,k+1)-E_x^n(i,j,k)}{\Delta z}\right] \end{aligned} \tag{4}$$

$$H_z^{n+1/2}(i,j,k) = \frac{1-\sigma^*\Delta t/2\mu}{1+\sigma^*\Delta t/2\mu}H_z^{n-1/2}(i,j,k) + \frac{\Delta t/\mu}{1+\sigma^*\Delta t/2\mu}\left[\frac{E_x^n(i,j+1,k)-E_x^n(i,j,k)}{\Delta y} - \frac{E_y^n(i+1,j,k)-E_y^n(i,j,k)}{\Delta x}\right] \quad (5)$$

$$E_x^{n+1}(i,j,k) = \frac{1-\sigma\Delta t/2\varepsilon}{1+\sigma\Delta t/2\varepsilon}E_x^n(i,j,k) + \frac{\Delta t/\varepsilon}{1+\sigma\Delta t/2\varepsilon}\left[\frac{H_Z^{n+1/2}(i,j,k)-H_z^{n+1/2}(i,j-1,k)}{\Delta y} - \frac{H_y^{n+1/2}(i,j,k)-H_y^{n+1/2}(i,j,k-1)}{\Delta z}\right] \quad (6)$$

$$E_y^{n+1}(i,j,k) = \frac{1-\sigma\Delta t/2\varepsilon}{1+\sigma\Delta t/2\varepsilon}E_y^n(i,j,k) + \frac{\Delta t/\varepsilon}{1+\sigma\Delta t/2\varepsilon}\left[\frac{H_x^{n+1/2}(i,j,k)-H_x^{n+1/2}(i,j,k-1)}{\Delta z} - \frac{H_z^{n+1/2}(i,j,k)-H_z^{n+1/2}(i-1,j,k)}{\Delta x}\right] \quad (7)$$

$$E_z^{n+1}(i,j,k) = \frac{1-\sigma\Delta t/2\varepsilon}{1+\sigma\Delta t/2\varepsilon}E_z^n(i,j,k) + \frac{\Delta t/\varepsilon}{1+\sigma\Delta t/2\varepsilon}\left[\frac{H_y^{n+1/2}(i,j,k)-H_y^{n+1/2}(i-1,j,k)}{\Delta x} - \frac{H_x^{n+1/2}(i,j,k)-H_x^{n+1/2}(i,j-1,k)}{\Delta y}\right] \quad (8)$$

In this work, the FDTD method with 10-cell thick UPML is used. The time step, Δt, is selected to satisfy 0.95 of Courant limit [17].

A corrugated surface is a metal slab, into which a series of vertical slots has been cut. The slots are narrow, so that many of them fit within one wave length across the slab. Each can be regarded as a parallel-plate transmission line, running down into the slab, and shorted at the bottom. If the slots are quarter-wave length deep, then the short circuit at the bottom end is transformed by the length of the slots into an open-circuit at the top end. Thus the impedance at the top surface is very high; the structure can be assigned efficient surface impedance equal to the total impedance of the slots [14].

3. NUMERICAL RESULTS

3.1. Reduced Coupling between Two Microstrip Elements

The mutual coupling $|S_{21}|$ between two coaxial fed microstrip antennas with infinite smooth ground plane has been calculated using the FDTD. The results are compared with the published measurements [18, 19]. The dimensions of the patch are: the patch length $L = 6.55\,\text{cm}$, patch width $W = 10.57\,\text{cm}$, substrate thickness $d = 0.1588\,\text{cm}$, the feed position at $x = 1.235\,\text{cm}$, and $y = 5.285\,\text{cm}$, the dielectric substrate material $\varepsilon_r = 2.55$ at resonant frequency $f_o = 1410\,\text{MHz}$ as shown in Fig. 1. The E-plane and the H-plane mutual coupling have been calculated versus the spacing (S/λ_o), the mutual coupling is calculated using the following equation:

$$S_{21}(f) = \frac{F(V_t)}{F(V_i)} \tag{9}$$

where V_i and V_t are the incident voltage pulse on port one and the transmitted voltage pulse on port two, respectively. $F(\ )$ is the fast Fourier Transform operator. At $f_o = 1410\,\text{MHz}$, the space steps used for FDTD are $\Delta x = 1.243\,\text{mm}$, $\Delta y = 1.235\,\text{mm}$, and $\Delta z = 0.5293\,\text{mm}$, and the number of iterations is 24,000 time step. Good agreement between the calculated and the measured results is observed as shown in Fig. 2 and Fig. 3 for the E-plane and the H-plane coupling, respectively. The E-plane coupling is larger due to stronger surface

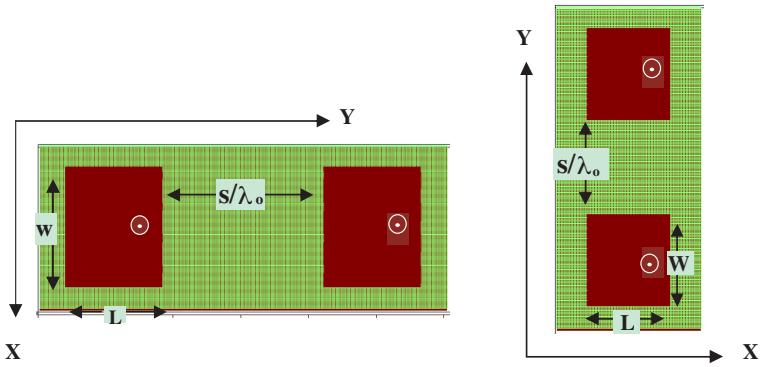

(a) The E-plane (b) The H-plane

Figure 1. Top view of two patch arrays antenna coaxial fed geometry at $f_o = 1410\,\text{MHz}$, $W = 10.57\,\text{cm}$, $L = 6.55$, $d = 0.1588$. Feed position ($y = 1.235\,\text{cm}$, $x = 5.285\,\text{cm}$).

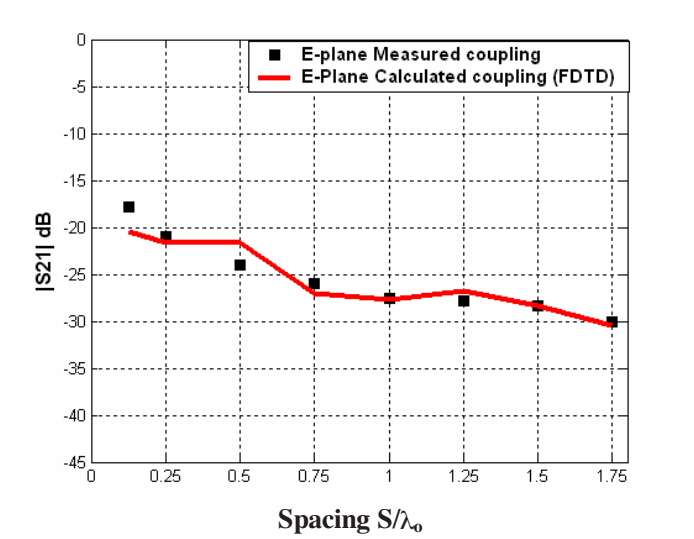

Figure 2. $|S_{21}|$ calculated using FDTD of the E-plane classic array antennas coaxial fed compared with the measured data [19] at f_o = 1410 MHz.

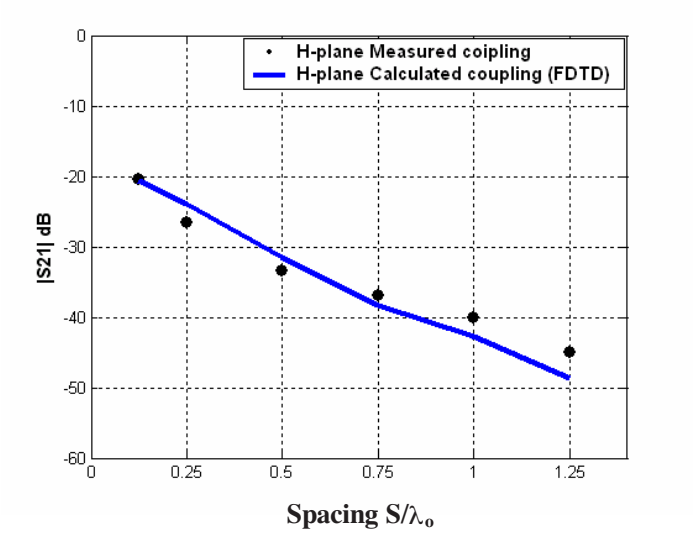

Figure 3. $|S_{21}|$ calculated using FDTD of the H-plane classic array antennas coaxial fed compared with the measured data [19] at f_o = 1410 MHz.

wave being excited compared to H-plane.

Based on [14, 15] and to reduce the mutual coupling between the two element array antennas, the space between the two element arrays is filled with corrugated ground surface. A corrugated ground surface is a metal slab, into which a series of vertical slots has been cut, as depicted in Fig. 4. The corrugation ground dimension is specified by the conductor slot width (groove width) $w_s = 0.1\lambda_o$, the ridge thickness $w_c = 0.03\lambda_o$, and the corrugation depth $h = \lambda_o/4$. The mutual coupling has been calculated versus the spacing between the elements ($0.25\lambda_o$, $0.5\lambda_o$, $0.75\lambda_o$ and λ_o only) for both the E-plane and the H-plane. The structure of the corrugation is changed as the spacing is increased. A reduction in the mutual coupling has been observed for the E-plane by 10.0 dB and 3.0 dB for the H-plane as shown in Fig. 5 and Fig. 6, respectively.

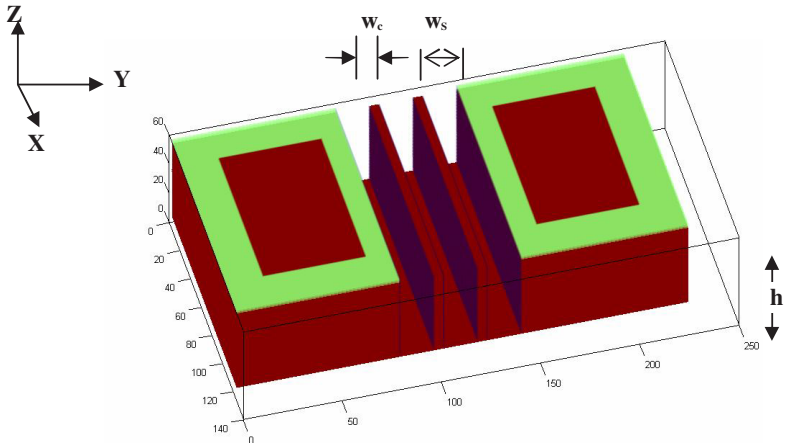

Figure 4. 3D Geometry of two element E-plane coaxial fed with corrugated ground surface, slot width (groove width) $w_s = 0.1\lambda_o$, the ridge thickness $w_c = 0.03\lambda_o$, and the corrugation depth $h = \lambda_o/4$ at 790 MHz.

3.2. Landmines Detection Sensor

Based on the previous section, two patches are constructed after scaling the frequency from $f_o = 1410$ MHz to $f_o = 790$ MHz at the UHF frequency. One of the patches is considered as the transmitting antenna and the second patch is considered as the receiving antenna. The sensor is located in air at certain height from the surface of the ground, while the soil has an electrical properties and the target is buried into the

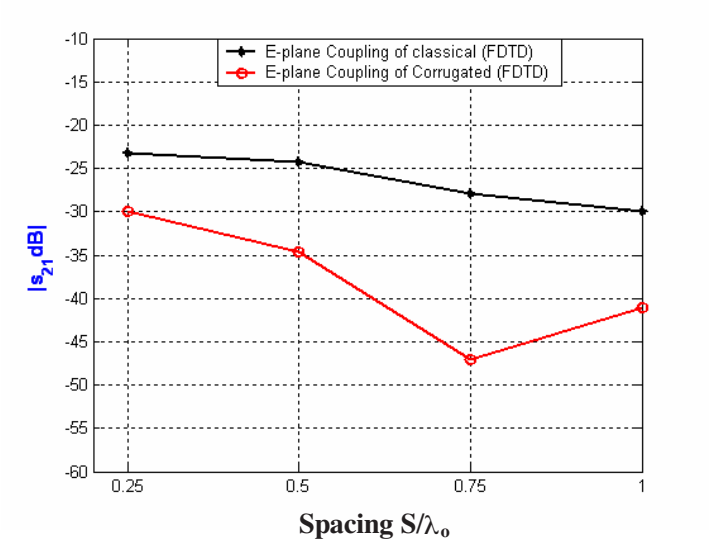

Figure 5. The calculated $|S_{21}|$, of the E-plane classic arrays coaxial fed and corrugated ground arrays.

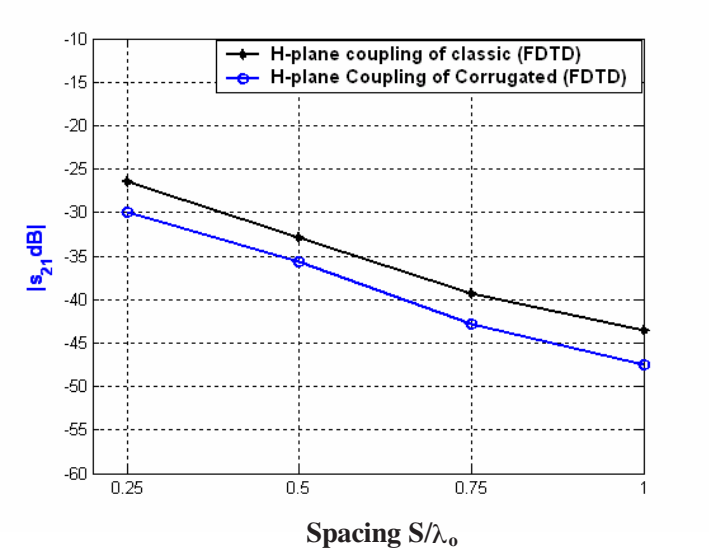

Figure 6. The calculated $|S_{21}|$, of the H-plane classic arrays coaxial fed and corrugated ground arrays.

soil with other different electrical properties whatever metallic target or nonmetallic target as shown in Fig. 7. When the sensor is moved over an empty soil, a small portion of signal will be reflected from the surface of the ground back to the receiving antenna, causing a small mutual coupling between the transmitting and the receiving antenna. When the sensor is moved over a soil containing a buried target, the target reflects a portion of the radiated signal by the transmitting antenna back to the receiving antenna, thus increasing the mutual coupling, and this coupling is used to detect the presence of buried targets.

The first sensor consists of two microstrip patch arrays elements (we call it classical sensor). Both patches are located on a smooth ground plane. The construction of the sensor and landmine is shown in Fig. 7(a) The space steps used for FDTD simulation at frequency $f_o = 790\,\text{MHz}$ step are $\Delta x = 1.7308\,\text{mm}$, $\Delta y = 1.6014\,\text{mm}$, and $\Delta z = 0.9415\,\text{mm}$. Each microstrip patch antenna consists of a rectangular patch with length $L = 116.9042\,\text{mm}$, patch width $w = 188.653\,\text{mm}$, substrate thickness $d = 2.8353\,\text{mm}$, the feed position $y = 33.629\,\text{mm}$, $x = 94.327\,\text{mm}$, and the spacing between the two patch is $\lambda_o/2 = 189.873\,\text{mm}$. The sensor with an infinite size ground plane is considered.

The second sensor consists of two microstrip patch with corrugated ground plane between the two patches at frequency $f_o = 790\,\text{MHz}$ (we call it corrugated sensor), each patch has length $L = 116.9042\,\text{mm}$, patch width $w = 188.653\,\text{mm}$, substrate thickness $d = 2.8353\,\text{mm}$, the feed position $y = 33.629\,\text{mm}$, $x = 94.327\,\text{mm}$ and the spacing between the two patch is $\lambda_o/2 = 189.873\,\text{mm}$. The corrugated ground plane is specified by slot width $w_s = 0.1\lambda_o = 37.9746\,\text{mm}$, the ridge thickness $w_c = 0.03\lambda_o = 11.3923\,\text{mm}$, while the depth is $h = \lambda_o/4 = 189.873\,\text{mm}$. The construction of the sensor and landmine is shown in Fig. 7(b).

3.3. Detecting Buried Targets

FDTD simulation has been carried out to calculate the detection capability of the two sensors under investigations. The first one is the classical sensor with smooth ground (classical Sensor), and the second is the sensor with corrugated ground plane (corrugated sensor). Different types of soil with different types of targets (mines) have been detecting using both sensors. FDTD simulations include the sensor construction, location in air, the soil properties and the buried target properties. The sensor is located in air at height $h = 2.8\,\text{cm}$, from the surface of the ground, while the target is buried at depth of $7.5\,\text{cm}$ under the ground inside the soil.

In the first case of our study the soil is described as "Fairly

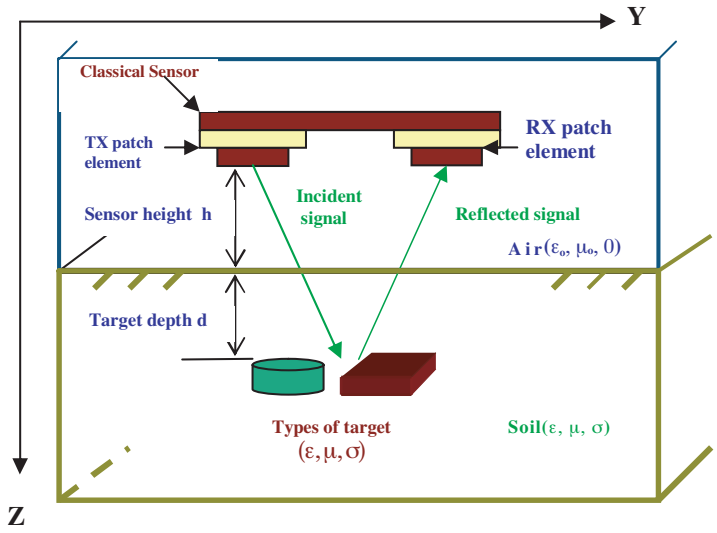

(a) Without corrugated ground

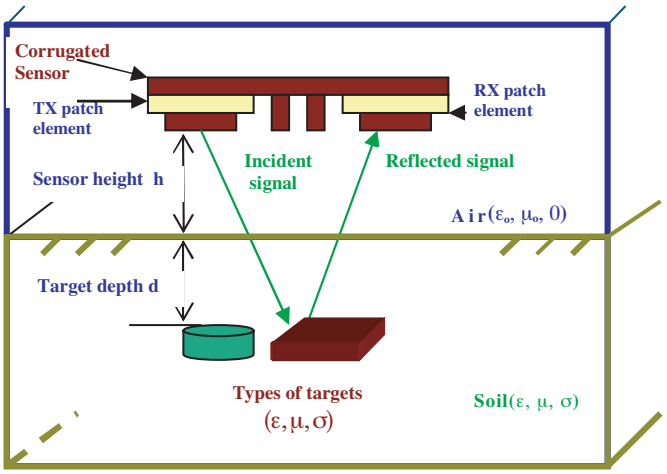

(b) With corrugated ground

Figure 7. Geometry of the whole problem for landmines detection, the domain includes the sensor in air at certain height (h) from the surface of the ground, the soil properties, and the target properties buried at depth (d).

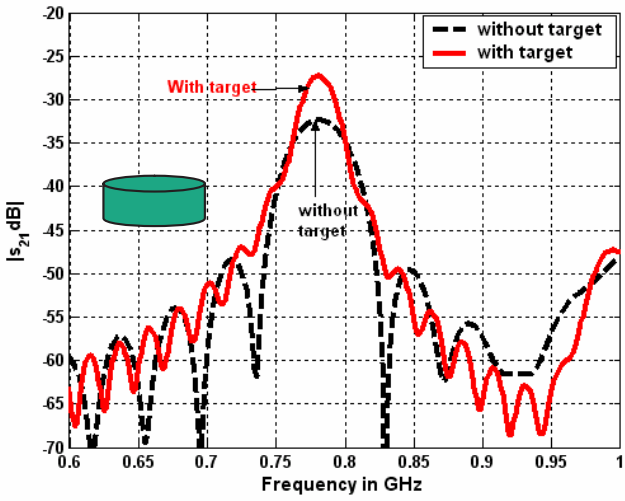

Figure 8. $|S_{21}|$ of classic sensor to detect circular Bakelite target buried in soil with $\varepsilon_r = 2.9$ at depth $d = 7.6$ cm, sensor height = 2.8 cm, using FDTD simulation at $f_o = 790$ MHz.

dry, loamy soil with moisture content by weight of 6%", with and electrical properties of $\varepsilon_r = 2.9$, $\mu_r = 1.0$, and $\sigma = 0.02$ S/m. Different types of buried targets have been detected inside the soil. The first buried target is PMN-mine (with relatively circular mine with bakelite body), its electrical properties is $\varepsilon_r = 4.5$, $\mu_r = 1.0$, $\sigma = 0.07$ s/m, weight = 550 g, its diameter = 110 mm, and height = 55 mm. A rubber membrane cover the top of the mine and is held in place by a thin metal band, whose diameter is 110 mm and 15 mm below the top of the target. The TNT material with electrical properties of $\varepsilon_r = 3.0$, $\mu = 1.0$, and $\sigma = 0.0029$ s/m. Fig. 8 shows the calculated mutual coupling, $|S_{21}|$, resulting from using the classical sensor in case of the absence the presence of the target is -30 dB and $-27.3.4$ dB, respectively. The difference between the two cases is about 2.0 dB. Fig. 9 shows the calculated mutual coupling, $|S_{21}|$, resulting from using the sensor with corrugated ground plane in case of the absence and presence of the target is -44.5 dB and -31.0 dB, respectively. The difference is about 13.5 dB. The corrugated ground plane enhanced the detection of the buried target by ~ 11 dB.

If the buried target in the same soil is circular metal target contains TNT material. The target characteristics are circular shape with diameter = 110 mm, height = 55 mm, weight = 550 g, and $\sigma = 58 \times 10^{12}$ s/m, while the TNT with electrical properties of $\varepsilon_r = 3.0$,

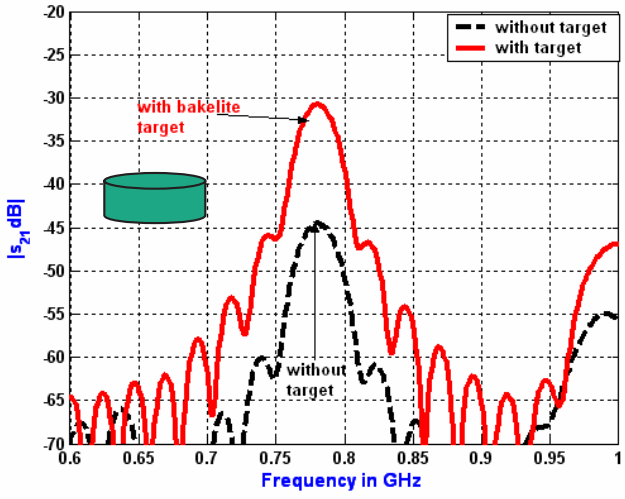

Figure 9. $|S_{21}|$ of sensor with corrugated ground to detect circular Bakelite target buried in soil with $\varepsilon_r = 2.9$ at depth $d = 7.6\,\text{cm}$, sensor height $= 2.8\,\text{cm}$, using FDTD simulation at $f_o = 790\,\text{MHz}$.

$\mu = 1.0$, and $\sigma = 0.0029\,\text{s/m}$, and weight $= 240\,\text{g}$. Fig. 10 shows the calculated mutual coupling, $|S_{21}|$, resulting from using the classical sensor in case of the absence the presence of the target is $-30\,\text{dB}$ and $-23.9.4\,\text{dB}$, respectively. The difference between the two cases is about $6.1\,\text{dB}$. Fig. 11 shows the calculated mutual coupling, $|S_{21}|$, resulting from using the sensor with corrugated ground plane in case of the absence and presence of the target is $-44.5\,\text{dB}$ and $-30.0\,\text{dB}$, respectively. The difference is about $14.5\,\text{dB}$. The corrugated ground plane enhanced the detection of the buried target by $\sim 12\,\text{dB}$.

If the buried target is a metal box target contains TNT material, the box dimensions are $(21 \times 20 \times 7\,\text{cm})$ into x, y, and z direction, respectively. The conductivity of the target is $\sigma = 58 \times 10^{12}\,\text{s/m}$. Fig. 12 shows the calculated mutual coupling, $|S_{21}|$, resulting from using the classical sensor in case of absence and presence of the target is $-30\,\text{dB}$ and $-27.4\,\text{dB}$, respectively. The difference between the two cases is about $2\,\text{dB}$. The calculated mutual coupling, $|S_{21}|$, resulting from using the sensor with corrugated ground plane is shown in Fig. 13. The mutual coupling in case of the presence and absence of the target are $-44.5\,\text{dB}$ and $-30.2\,\text{dB}$, respectively. The difference is about $-14\,\text{dB}$. The corrugated ground plane enhanced the detection of the buried target by $\sim 12\,\text{dB}$.

In the Second case of our study The soil is described as "Red

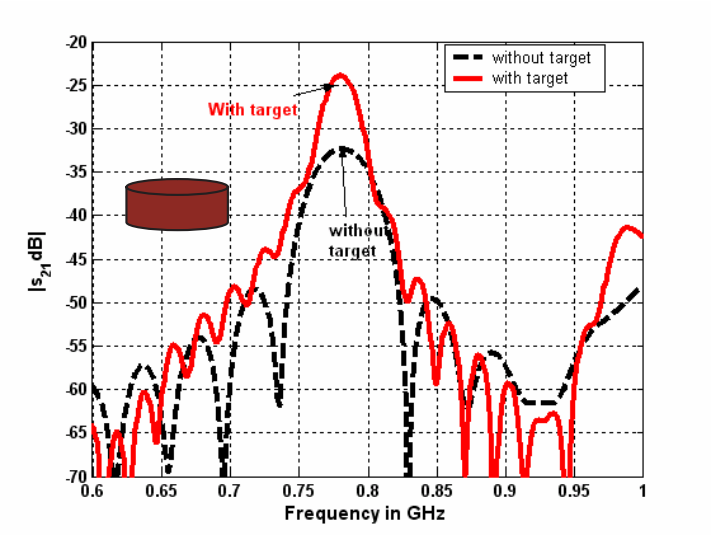

Figure 10. $|S_{21}|$ of classic sensor to detect circular metal target buried in soil with $\varepsilon_r = 2.9$ at depth $d = 7.6\,\text{cm}$, sensor height $= 2.8\,\text{cm}$, using FDTD simulation at $f_o = 790\,\text{MHz}$.

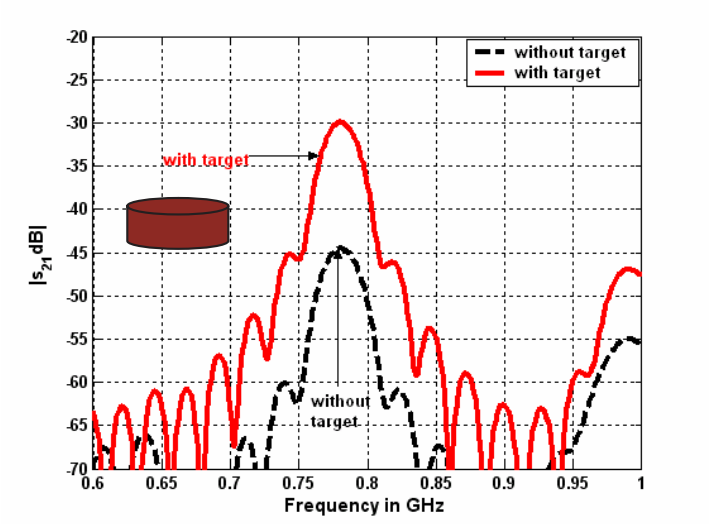

Figure 11. $|S_{21}|$ of sensor with corrugated ground to detect circular metal target buried in soil with $\varepsilon_r = 2.9$ at depth $d = 7.6\,\text{cm}$, sensor height $= 2.8\,\text{cm}$, using FDTD simulation at $f_o = 790\,\text{MHz}$.

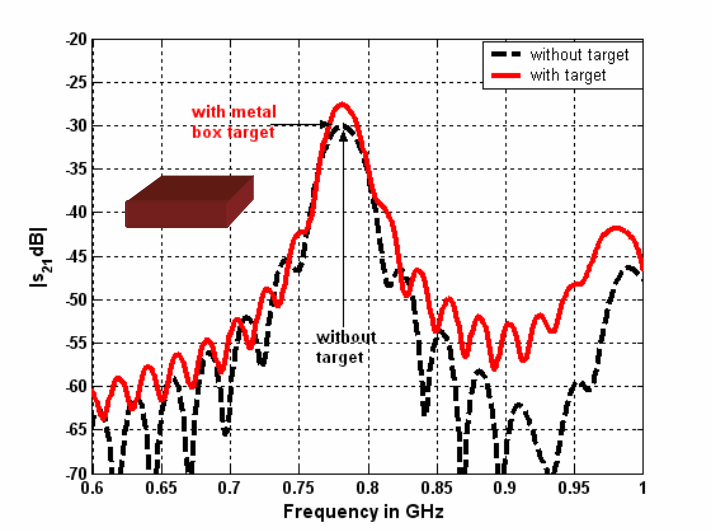

Figure 12. $|S_{21}|$ of classic sensor to detect metal box target buried in soil with $\varepsilon_r = 2.9$ at depth $d = 7.6\,\text{cm}$, sensor height $= 2.8\,\text{cm}$, using FDTD simulation at $f_o = 790\,\text{MHz}$.

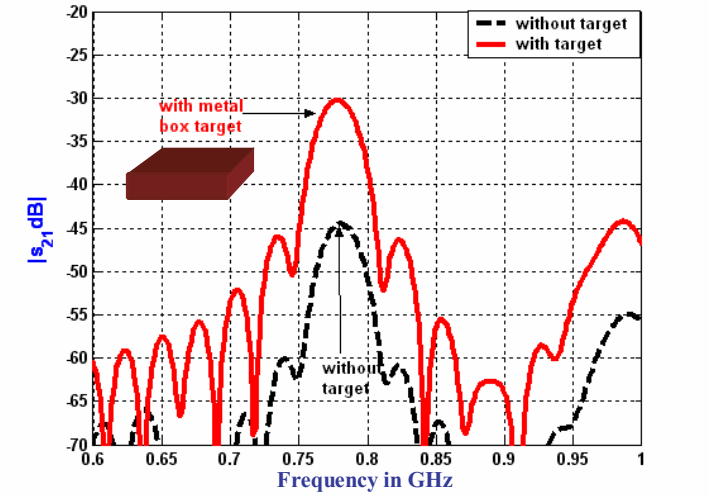

Figure 13. $|S_{21}|$ of sensor with corrugated ground to detect metal box target buried in soil with $\varepsilon_r = 2.9$ at depth $d = 7.6\,\text{cm}$, sensor height $= 2.8\,\text{cm}$, using FDTD simulation at $f_o = 790\,\text{MHz}$.

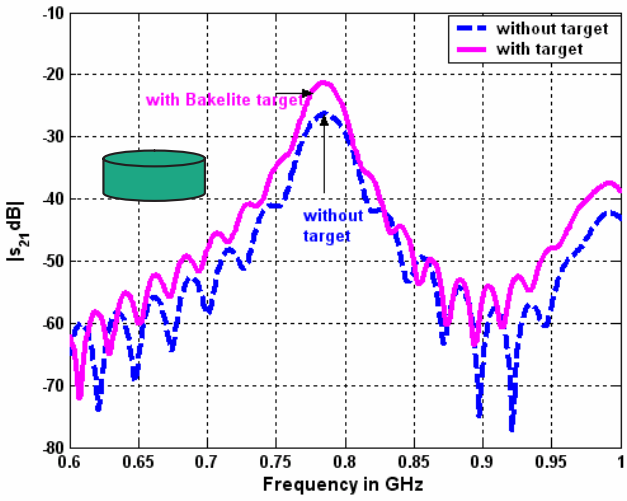

Figure 14. $|S_{21}|$ of classic sensor to detect circular Bakelite target buried in soil with $\varepsilon_r = 8.1$ at depth $d = 7.6$ cm, sensor height $= 2.8$ cm, using FDTD simulation at $f_o = 790$ MHz.

clay with 9.6% water and dry weight", with and electrical properties of $\varepsilon_r = 8.1$, $\mu_r = 1.0$, and $\sigma = 0.038$ s/m. All the different targets in the first case of study will also be detect in the second case of study. In case of detecting the circular bakelite target with electrical properties mentioned above. Fig. 14 shows the calculated mutual coupling, $|S_{21}|$, resulting from using the classical sensor in case of absence and presence of the target is -26.32 dB and -21.3 dB, respectively. The difference between the two cases is about 5.02 dB. Fig. 15 shows the calculated mutual coupling, $|S_{21}|$, resulting from using the sensor with corrugated ground plane in case of absence and presence of the target are $-50.6.5$ dB and -41.3 dB, respectively. The difference is about 9.3 dB. The corrugated ground plane enhanced the detection of the buried target by ~ 4.5 dB.

If the buried target in the soil is circular metal target with TNT material, with the same pervious properties as mentioned above in the first case study, Fig. 16 shows the calculated mutual coupling, $|S_{21}|$, resulting from using the classical sensor in case of absence and presence of the target is -26.32 dB and -19.23 dB, respectively. The difference between the two cases is about 7.0 dB. Fig. 17 shows the calculated mutual coupling, $|S_{21}|$, resulting from using the sensor with corrugated ground plane in case of absence and presence of the target are $-50.6.5$ dB and 38 dB, respectively. The difference is about 12.6 dB.

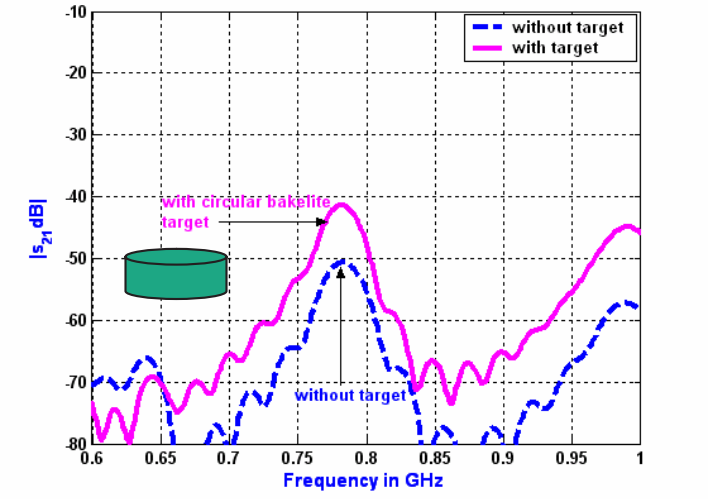

Figure 15. $|S_{21}|$ of sensor with corrugated ground to detect circular Bakelite target buried in soil with $\varepsilon_r = 8.1$ at depth $d = 7.6\,\text{cm}$, sensor height $= 2.8\,\text{cm}$, using FDTD simulation at $f_o = 790\,\text{MHz}$.

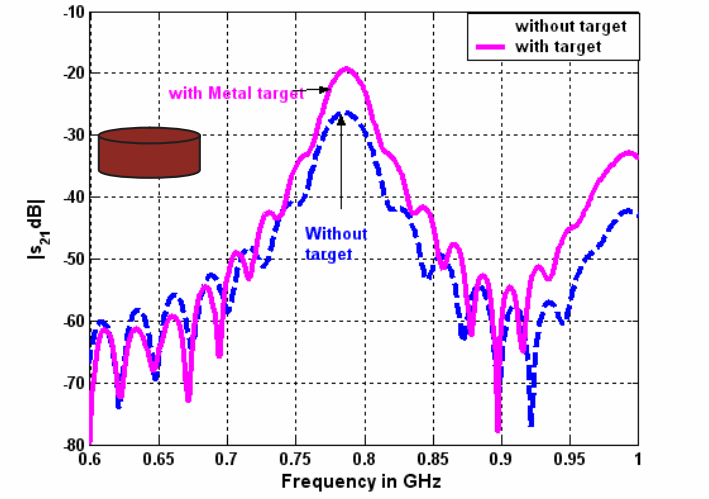

Figure 16. $|S_{21}|$ of classic sensor to detect circular metal target buried in soil with $\varepsilon_r = 8.1$ at depth $d = 7.6\,\text{cm}$, sensor height $= 2.8\,\text{cm}$, using FDTD simulation at $f_o = 790\,\text{MHz}$.

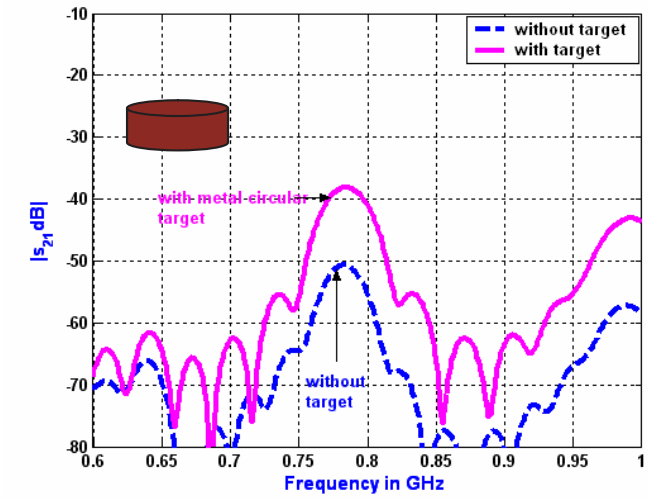

Figure 17. $|S_{21}|$ of sensor with corrugated ground to detect circular metal target buried in soil with $\varepsilon_r = 8.1$ at depth $d = 7.6\,\text{cm}$, sensor height $= 2.8\,\text{cm}$, using FDTD simulation at $f_o = 790\,\text{MHz}$.

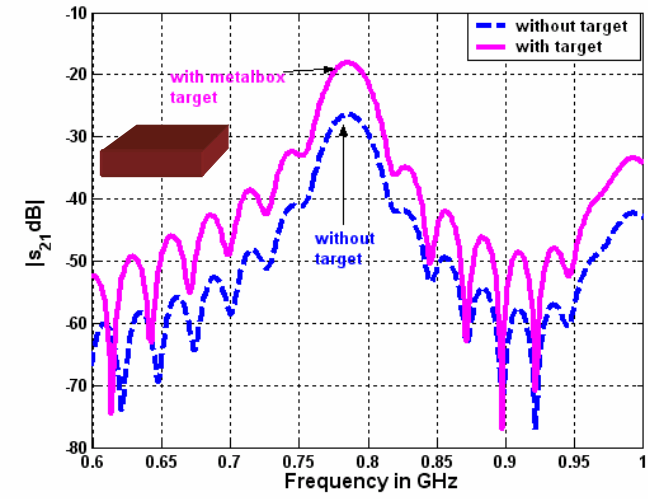

Figure 18. $|S_{21}|$ of classic sensor to detect metal box target buried in soil with $\varepsilon_r = 8.1$ at depth $d = 7.6\,\text{cm}$, sensor height $= 2.8\,\text{cm}$, using FDTD simulation at $f_o = 790\,\text{MHz}$.

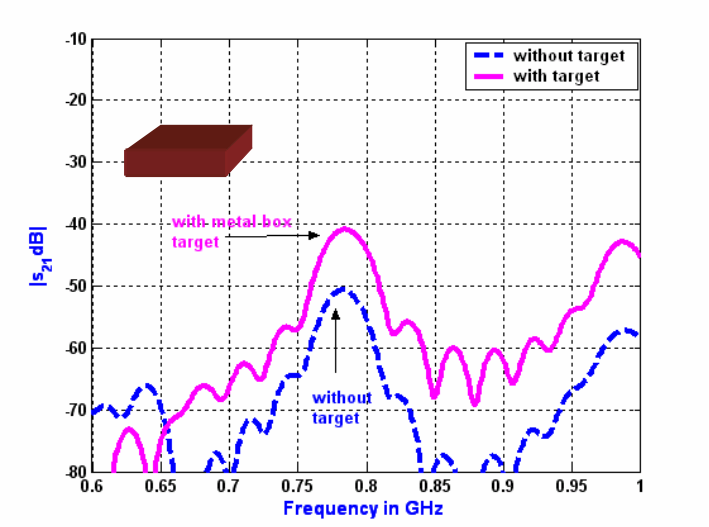

Figure 19. $|S_{21}|$ of sensor with corrugated ground to detect metal box target buried in soil with $\varepsilon_r = 8.1$ at depth $d = 7.6\,\text{cm}$, sensor height $= 2.8\,\text{cm}$, using FDTD simulation at $f_o = 790\,\text{MHz}$.

Again, the corrugated ground plane enhanced the detection of the buried target by $\sim 6\,\text{dB}$.

If the buried target is a metal box target contains TNT material, with the same previous electrical properties, Fig. 18 shows the calculated mutual coupling, $|S_{21}|$, resulting from using the classical sensor in case of absence and presence of the target is $-26.32\,\text{dB}$ and $-18.0\,\text{dB}$, respectively. The difference between the two cases is about $8.32\,\text{dB}$. Fig. 19 shows the calculated mutual coupling, $|S_{21}|$, resulting from using the sensor with corrugated ground plane. The mutual coupling in case of the presence and absence of the target are $-50.6\,\text{dB}$ and $-40.8\,\text{dB}$, respectively. The difference is about $9.8\,\text{dB}$. The corrugated ground plane enhanced the detection of the buried target by $\sim 2\,\text{dB}$.

4. CONCLUSION

The FDTD simulation has been used to simulate the detection process of the buried targets using a new proposed sensor. It consists of two parallel microstrip antennas that are placed on same ground plane with corrugated ground surface between the arrays. The proposed sensor has the advantage of low mutual coupling between the elements of

the array and improved detecting capability compared with classical sensor. The detecting capability depends on the types of the soil and targets.

REFERENCES

1. Boutros-Ghali, B., "The land mine crisis," *Foreign Affairs*, Vol. 73, 8–13, Sept.–Oct. 1994.
2. Brooks, J., "The detection of buried non-metallic anti-personal landmines," Ph.D. Dissertation, The University of Alabama in Huntsville, Huntsville, Alabama, 2000.
3. Guo, B., Y. Wang, J. Li, P. Stoica, and R. Wu, "Microwave imaging via adaptive beam forming methods for breast cancer detection," *J. of Electromagn. Waves and Appl.*, Vol. 20, No. 1, 53–63, 2006.
4. Van den Bosch, I., S. Lambot, M. Acheroy, I. Huynen, and P. Druyts, "Accurate and efficient modeling of monostatic GPR signal of dielectric targets buried in stratfield media," *J. of Electromagn. Waves and Appl.*, Vol. 20, No. 3, 283–290, 2006.
5. Chen, X., D. Liang, and K. Huang, "Microwave imaging 3-D buried objects using parallel genetic algorithm combined with FDTD technique," *J. of Electromagn. Waves and Appl.*, Vol. 20, No. 13, 1761–1774, 2006.
6. Xue, W. and X.-W. Sun, "Target detection of vehicle volume detection Radar based on Winger-Hough transform," *J. of Electromagn. Waves and Appl.*, Vol. 21, No. 11, 1513–1523, 2007.
7. Bourgeois, J. M. and G. S. Smith, "A full electromagnetic simulation of a ground penetrating radar: Theory and experiment," *IEEE Antenna Propagat. S. Int. Symp. Dig.*, Vol. 32, 1442–1445, June 1994.
8. Bourgeois, J. M. and G. S. Smith, "A complete electromagnetic simulation of a ground penetrating radar for mine detection: theory and experiment," *IEEE Antenna Propagat. S. Int. Symp. Dig.*, Vol. 35, 986–989, June 1997.
9. Bourgeois, J. M. and G. S. Smith, "A complete electromagnetic simulation of the separated-aperture sensor for detecting buried landmines," *IEEE Trans. Antennas Propagat.*, Vol. AP-46, 1419–1426, Oct. 1998.
10. Zainud-Deen, S. H., M. E. Badr, K. H. Awadalla, and H. A. zSharshar, "Microstrip antenna for detecting buried landmines," *23rd NRSC2006 Symp.*, Faculty of Electronic Engineering, Menoufya, Univ. Egypt, March 14–16, 2006.

11. Zainud-Deen, S. H., M. E. Badr, K. H. Awadalla, and H. A. Sharshar, "Microstrip antenna with shorting Pins as a Sensor for landmines detecting," *24th NRSC2007 Symp.*, Faculty of Engineering, Ain Shams, Univ. Cairo, Egypt, March 13–15, 2007.
12. Nikolic, M. M., R. A. Djordevic, and A. Nehorai, "Microstrip antennas with suppressed radiation in horizontal directions and reduced coupling," *IEEE Trans. Antennas Propagat.*, Vol. AP-53, No. 11, 3469–3476, Nov. 2005.
13. Yook, J. G. and L. Katchi, "Micro machined microstrip antenna with controlled mutual coupling and surface waves," *IEEE trans. Antennas Propagat.*, Vol. AP-49, 1282–1289, Sep. 2001.
14. Sievenpiper, D. F., "High-impedance electromagnetic surface," Ph.D. Dissertation, University of California, Los Angels, 1999.
15. El-Deen, E. and M. Aly, "Analysis of electromagnetic waves in the Time domain," MSc. Thesis, Faculty of Electronic Engineering, University Egypt, Menoufia, 2006.
16. Yee, K. S., "Numerical solution of initial boundary value problems involving Maxwell's equations in isotropic media," *IEEE Trans. Antennas Propagat.*, Vol. AP-14, 302–307, 1966.
17. Taflove, A., *Computational Electrodynamics: The Finite Difference Time Domain Method*, Artech House, Norwood, MA, 2000.
18. Jeddicka, R. P., M. T. Poe, and R. Carver, "Measured mutual coupling between microstrip antennas," *IEEE Trans. Antennas Propagat.*, Vol. AP-29, 147–149, 1981.
19. Pozar, D. M., "Input impedance and mutual coupling of rectangular microstrip antennas," *IEEE Trans. Antennas Propagat.*, Vol. AP-30, 1191–1196, 1982.